Variable in-situ stress orientations across the northern Hikurangi Subduction Margin

McNamara, D. D.[1], Behboudi, E.[2], Wallace, L.[3,4], Saffer, D.[4], Cook, A. E.[5], Fagereng, A.[6], Paganoni, M.[7], Hung-Yu, W.[8], Kim, G.[9], Lee, H.[9], Savage, H. M.[10], Barnes, P.[11], Pecher, I.[12], LeVay, L. J.[13], Petronotis, K. E.[13]

Keywords: stress orientation; borehole image; borehole breakout; logging while drilling; Hikurangi Subduction Margin

[1] Department of Earth, Ocean and Ecological Sciences, University of Liverpool, U.K.

[2] Irish Centre for Research in Applied Geoscience, University College Dublin, Ireland

[3] GNS Science, New Zealand

[4] University of Texas Institute for Geophysics, Austin, TX, U.S.A.

[5] School of Earth Sciences, Ohio State University, U.S.A.

[6] School of Earth and Ecological Sciences, Cardiff University, U.K.

[7] University of Oxford, U.K.

[8] Department of Resources Engineering, National Cheng Kung University, Taiwan

[9] Korea Institute of Geoscience and Mineral Resources (KIGAM), Republic of Korea

[10] Department of Earth and Planetary Sciences, University of California, Santa Cruz, U.S.A.

[11] National Institute of Water and Atmospheric Research (NIWA), New Zealand

[12] School of Environmental and Marine Sciences, University of Auckland, New Zealand

[13] International Ocean Discovery Program, Texas A&M University, U.S.A.

Keywords

Slow slip earthquakes, borehole image logs, borehole breakouts, stress orientation, subduction, Hikurangi

Abstract

We constrain the orientation of the horizontal stress field from borehole image data in a transect across the Hikurangi Subduction Margin. This region experiences NW-SE convergence leading to recurrent slow slip events. The direction of the horizontal maximum stress is E-W at an active thrust fault near the subduction margin trench. This trend changes to NNW-SSE in the Tuaheni Basin in the offshore accretionary wedge, and to NE-SW in the onshore forearc. Multiple, tectonic and geological processes, either individually or in concert, may explain this variability. A general offshore-onshore stress rotation may reflect a change from dominantly compressional tectonics at the deformation front, to a strike-slip and/or extensional stress regime closer to the Taupo Volcanic Zone. In addition, the offshore stress may be affected by topography and/or stress rotation around subducting seamounts, and/or temporal stress changes during the slow slip cycle.

Plain Language Summary

Using geophysical images captured from the inside of boreholes drilled across the Hikurangi Subduction Margin, an area that experiences slow earthquakes, we describe variability in the direction of modern day maximum horizontal tectonic forces (stress) at this collisional plate boundary. Changes in the direction of maximum horizonal stress occur as you move from the plate boundary toward the onshore region of New Zealand's North Island. We provide a range of possible tectonic and geological processes that either individually or in concert may explain our observed stress direction variations. This includes changing tectonic regimes as you move away from the plate boundary, topography, and effects on the stress field caused by the presence of subducting seamounts, and changing stress conditions related to the intermittent activity of slow earthquakes.

1) Maximum horizontal stress directions vary in a transect across the Hikurangi Subduction Margin
2) Stress orientations suggest a change occurs moving from offshore to onshore associated with changing dominant tectonic regime
3) Offshore stress variation may be caused by a number of specific tectonic and geological causes.

1 Introduction

The stress state in the crust is a fundamental control on a wide range of processes, including crustal deformation, earthquake dynamics, the generation and maintenance of topography, and crustal hydrology (Duan, 2010; Ito & Zoback, 2000; Miller & Dunne, 1996; Sibson et al., 2011; Warren-Smith et al., 2019; Zoback & Townend, 2001). Fault slip resulting from stress accumulation is a function of the orientation and magnitudes of the three principal stresses (σ_1, σ_2, σ_3), subsurface pore pressures (P_p), orientations of existing faults, and rock cohesion and friction (Anderson, 1906; Zoback et al., 1989). Stress orientations, magnitudes, and pore pressures can in turn be altered by local topography, mechanical contrasts of geological units in the subsurface, and earthquake and creep activity. Studies of active tectonic systems, including shallow subduction zones, reveal both temporal and spatial perturbations in the crustal stress state related to fault geometry and activity (Byrne et al., 2009; Chang et al., 2010; Hardebeck & Okada, 2018; Lin et al., 2009; McNamara et al., 2015), earthquake slip (Allmann & Shearer, 2009; Brodsky et al., 2017; Lin et al., 2015), and redistribution of pore pressure (Magee & Zoback, 1993; Song et al., 2011).

Episodic, shallow (<15 km) slow slip events, spanning timescales ranging from days to years, are recorded at several subduction zones, including the Nankai margin, offshore Japan (Araki et al., 2017; Hirose et al., 1999; Obara et al., 2004), the Costa Rican margin (Davis et al., 2015; Dixon et al., 2014), and the Hikurangi Subduction Margin (HSM) (Wallace et al., 2012, 2016). Despite the recognised importance of stress in earthquake dynamics, data constraining stress states and stress variability on, and in the near field of, faults that host slow slip earthquakes (SSEs) is limited (Chang et al., 2010; Huffman et al., 2016; Warren-Smith et al., 2019). This study provides new data on contemporary stress orientation variability across an area of recurring slow slip in the northern HSM. We characterise shallow crustal stress orientations from boreholes along a transect from the actively deforming frontal accretionary wedge, through the landward, offshore Tuaheni Basin, and onto the onshore forearc (Figure 1). We then discuss possible geological processes responsible for the observed stress orientation variations.

1.1 State of Stress at the Hikurangi Subduction Margin

The HSM accommodates westward subduction of the Pacific plate beneath the North Island of New Zealand (Australian Plate) at rates of ~2-3 cm/year in the south, and ~6 cm/year in the north (Figure 1a) (Wallace et al., 2004). Changes in subduction rate relate to clockwise rotation of the forearc which creates changes in upper plate tectonics along-strike of the margin. Pacific-Australia plate convergence is oblique, with the margin-perpendicular component accommodated primarily along shallow subduction thrust faults, and the margin-parallel component accommodated by a combination of forearc rotation and strike-slip tectonics in the onshore North Island Dextral Fault Belt (NIDFB) (Beanland & Haines, 1998; Wallace et al., 2004).

Episodic SSEs are observed at shallow depths of 2-15 km at the northern HSM every 18 to 24 months, and involve >20 cm of slip on the plate boundary occurring over a 1-2-week period (Wallace et al., 2010, 2016). There have also been moderate-sized subduction thrust earthquakes in the north Hikurangi SSE source region, including two Mw 7.0-7.2 events in 1947 (Figure 1c) (Doser & Webb, 2003).

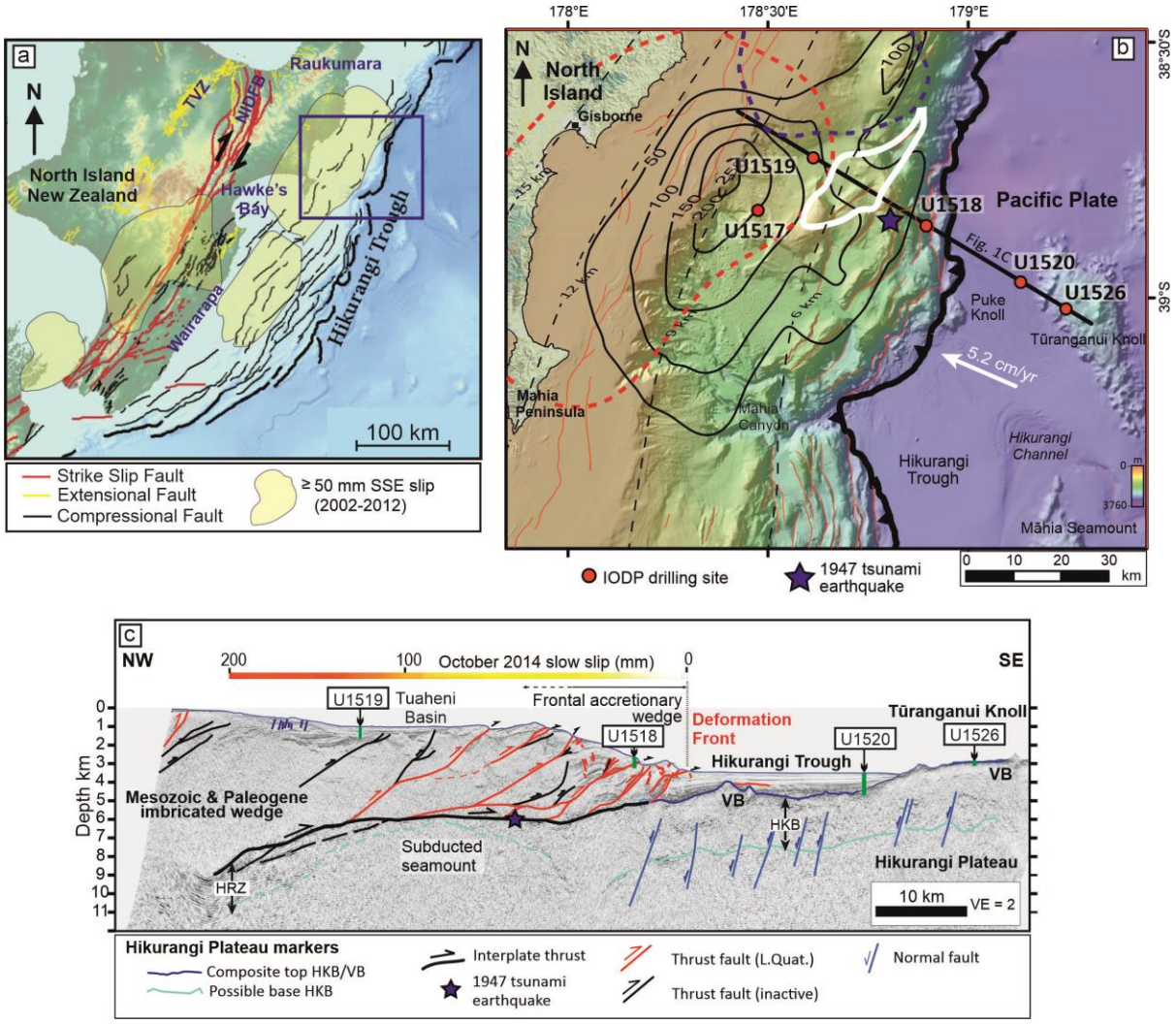

Figure 1. a) Map of the North Island of New Zealand, tectonic structures, and the extent of regions that have experienced cumulative slow slip of ≥50 mm between 2002-2012 (Wallace & Eberhart-Phillips, 2013). Fault traces from (Barnes et al., 2010; Langridge et al., 2016; Mountjoy & Barnes, 2011; Pedley et al., 2010); blue square is the area depicted in Figure 1b. b) Bathymetric map showing the location of IODP Expeditions 372 and 375 drill Sites (U1517, U1519, U1518, U1520, and U1526), and the seismic line 05CM-04 (Figure 1c). Modified from (Barnes et al., 2020) the figure shows the extent of three recent SSEs (fine black lines with labels are slip contours (mm) for the September to October 2014 SSE, blue dashed lines are 40-mm slip contours for the January to February 2010 SEE, and red dashed line is the 40-mm slip contour for the March to April 2010 SEE (Wallace et al., 2016), dashed black lines show the approximate depth of the plate interface (Williams et al., 2013), bold black line with teeth marks the plate boundary deformation front, fine red lines are upper plate thrust fault traces, the bold white line is the approximate morphology of an inferred subducted seamount (Barker et al., 2018). c) Interpretation of NW-SE seismic profile 05CM-04 (modified from (Barnes et al., 2020)), showing the interpreted location of major structures, and well locations (green lines). Coloured scale shows amount of slip across the HSM during the 2014 SEE (Wallace et al., 2016).

Some aspects of the HSM stress state have been reported previously. For example, at the northern HSM, focal mechanism-derived S_{Hmax} directions are NE-SW (oblique to relative plate motion, and oriented approximately parallel to the strike of the margin), with some suggested local variation in the area east of Gisborne where ENE-WSW S_{Hmax} directions are noted (subparallel to relative plate motion, and strike-oblique) (Townend et al., 2012). Borehole image logs (acquired within the upper 3 km of the crust) from three onshore wells also show NE-SW S_{Hmax} orientations in the Hawke's Bay region (Lawrence, 2018). Investigations of principal contraction (strain) directions from GPS measurements along the HSM are highly variable, with dominantly east-west directions near the east coast, and with some principal contraction directions rotating to NE-SW further inland (Dimitrova et al., 2016; Haines & Wallace, 2020).

Pore pressure (P_p) measured from drill stem tests and repeat formation testing, and inferred from mud weights in onshore wells, reveal shallow overpressures within basins of the upper plate (Burgreen-Chan et al., 2016; Darby and Funnell, 2001). The Hawke's Bay region displays lower overpressures than Raukumara and northern Hawke's Bay. Overpressures are found within Cretaceous to Paleogene lithostratigraphic units, are spatially variable within Neogene units, and uncommon within Quaternary units (Darby & Funnell, 2001). These shallow overpressures have been attributed to both disequilibrium compaction, where pore water flow is restricted during sediment compaction, and to porosity reduction associated with high horizontal compressive stresses related to plate convergence (Burgreen-Chan et al., 2016; Darby & Funnell, 2001). Finally, in the Hawke's Bay region, σ_3 magnitudes determined from leak-off tests performed in onshore wells are less than (though in places close to) vertical stress (S_v) magnitudes, consistent with a strike-slip or reverse faulting stress regime, where σ_3 is the horizontal minimum stress (S_{hmin}) or the S_v respectively (Burgreen-Chan et al., 2016).

2 Methods and Data

2.1 GVR resistivity image log processing and analysis

International Ocean Discovery Program (IODP) Expeditions 372/375 drilled a series of wells across the HSM (Saffer et al., 2019b) (Figure 1). As part of Expedition 372, a suite of LWD data including geoVISION (GVR) resistivity image logs were acquired in Holes U1517A, U1518A/B, U1519A, and U1520A/B. Hole U1517A was drilled through bedded, clayey-silt sediment packages associated with the Tuaheni Landslide Complex (Pecher et al., 2019). Hole U1518A/B drilled across the Pāpaku Fault, an active splay thrust fault in the frontal accretionary wedge, and the bedded sediments that comprise its hangingwall and footwall (Fagereng et al., 2019; Wallace et al., 2018). Hole 1519A is located ~38km offshore within an upper continental slope sedimentary basin (Tuaheni Basin) and intersects bedded mudstones, siltstones, and sandstone packages, as well as mass transport deposits (Saffer et al., 2019b). Finally, Hole U1520A/B is located on the incoming subducting plate and intersects

the trench-wedge clastic sediments and a lower sequence of carbonates and volcaniclastics (Barnes et al., 2020).

GVR resistivity image logs are analysed in this study to identify and quantify the properties of natural structures (fractures) and stress-induced borehole features such as borehole breakouts. GVR logging provides a 360° image of the borehole wall. This study reports borehole breakout orientation results determined from a high-resolution, post-expedition reanalysis of the GVR image logs which have resulted in a more detailed and accurate data set in comparison to the preliminary data provided from the shipboard analysis (Wallace et al., 2018). Raw data was processed from the GVR tool following the procedure detailed in (Wallace et al., 2019). For this study all GVR images (those generated from the shallow, medium, and deep resistivity button) were analysed. The shallow button GVR image logs are the preferred image for data acquisition as they have a higher potential of recording features close to the borehole wall, including stress-induced features such as borehole breakouts and drilling-induced tensile fractures (DITF). The GVR image logs were statically and dynamically normalised to enhance resistivity contrast for improved feature identification, with a 1 m and 0.5 m normalisation window used for the latter. Feature classification is based on criteria set out in (McNamara et al., 2019). Quality rankings and circular statistics for stress induced borehole features identified from the GVR image logs follow World Stress Map criteria (Heidbach, 2016).

3 Results

3.1 Borehole Image Stress Induced Features

From all GVR image logs collected during IODP Expedition 372, 82 distinct borehole breakout pairs are identified in Holes U1518A/B and U1519A; none were identified within the other Holes (Table 1; Figure 2). No drilling-induced tensile fractures, or petal centreline fractures are observed on resistivity image logs at any of the drill sites. Borehole breakout azimuths are variable between the two drillsites and with depth in each individual Hole (Figure 2).

Eight of the ten borehole breakout pairs identified in Hole U1518B occur between 518-591 mbsf (metres below seafloor) and have an average orientation of 003°±6° / 180°±4° (Figure 2a). These lie in the footwall of the Pāpaku fault that was intersected at 315-348 mbsf (Cook et al., 2020). From these breakout orientations we report an S_{hmin} orientation of N-S, and infer an S_{Hmax} orientation of E-W (Figure 2a, 2b). Orientation trend variations between borehole breakouts <10 m apart range between 3° and 16° within this interval (Figure 2a). In the hanging wall (~210-220 mbsf), two borehole breakout pairs (low resistivity zones, approximately 180° apart around the borehole, associated with an increase in caliper values) are identified and have 065°/252° and 056°/236° azimuths (Figure 2a), from which a NE-SW S_{hmin} and NW-SE S_{Hmax} orientation is inferred.

At Hole U1519A, 72 borehole breakout pairs have average azimuths of 072°/±13° / 252°/±9° (Table 1), corresponding to an ENE-WSW S_{hmin} and NNW-SSE S_{Hmax} orientation (Figure 2c, 2d). Most borehole breakouts cluster within two depth intervals, 596-616 mbsf (cluster A) and 640-661 mbsf (cluster B) (Figure 2c). Localised variation of borehole breakout azimuth (between borehole breakouts <10 m apart) ranges from <1° to 52° (average variation of 12°±9°) (Figure 2c). The largest of these azimuth variations (52°) occurs at ~545 mbsf and includes a borehole breakout azimuth (029°) that sits outside the circular statistical range for Hole U1519A (Figure 2c). Both clusters show a maximum borehole breakout azimuth variation of 31° at 607.5 mbsf (cluster A) and 658.5 mbsf (cluster B).

Hole	**U1518B**	**U1519A**
Latitude	38°51.5476'S	38°43.6372'S
Longitude	178°53.7621'E	178°36.8537'E
Average Borehole Breakout Azimuth (°)	003 / 180	072 / 252
S.D. (°)	4 / 6	9 / 13
Feature Type	Borehole Breakout	Borehole Breakout
n	10	73
Total Length of Borehole Breakouts (m)	2.2	16.8 - 17.3
Stress Indicator Quality Ranking	A	A
Date of Image Logging	21st December 2017	24th December 2017
Top Borehole Breakout Depth (mbsf / mrsl)	210 / 2844	28 / 1028
Bottom Borehole Breakout Depth (mbsf / mrsl)	591 / 3225	661 / 1662
Sea Floor Depth (mrsl)	2634.6	1000.7
Distance Between Rig Floor and Sea Level (m)	10.9	10.9
Image Log Top (mbsf / mrsl)	54.5 / 2689.1	92 / 1092.7
Image Log Bottom (mbsf / mrsl)	647.1 / 3281.7	755.8 / 1756.5
Well Orientation	Vertical	Vertical

Table 1. Stress indicators from analysed LWD resistivity image from IODP Expedition 372. Average borehole breakout azimuths and standard deviations (S.D.) calculated according to World Stress Map criteria (Mardia, 1975; Tingay et al., 2008) and show values generated for both pairs of borehole breakout sets. N = number of borehole breakout pairs. Stress indicator quality ranking based solely on standard deviations of the borehole breakout azimuths and do not account for length component of quality laid out by the World Stress Map Project (Tingay et al., 2008) due to conflicting aspects of the quality criteria for this dataset. mrsl = metres relative to sea level; mbsf = meters below seafloor.

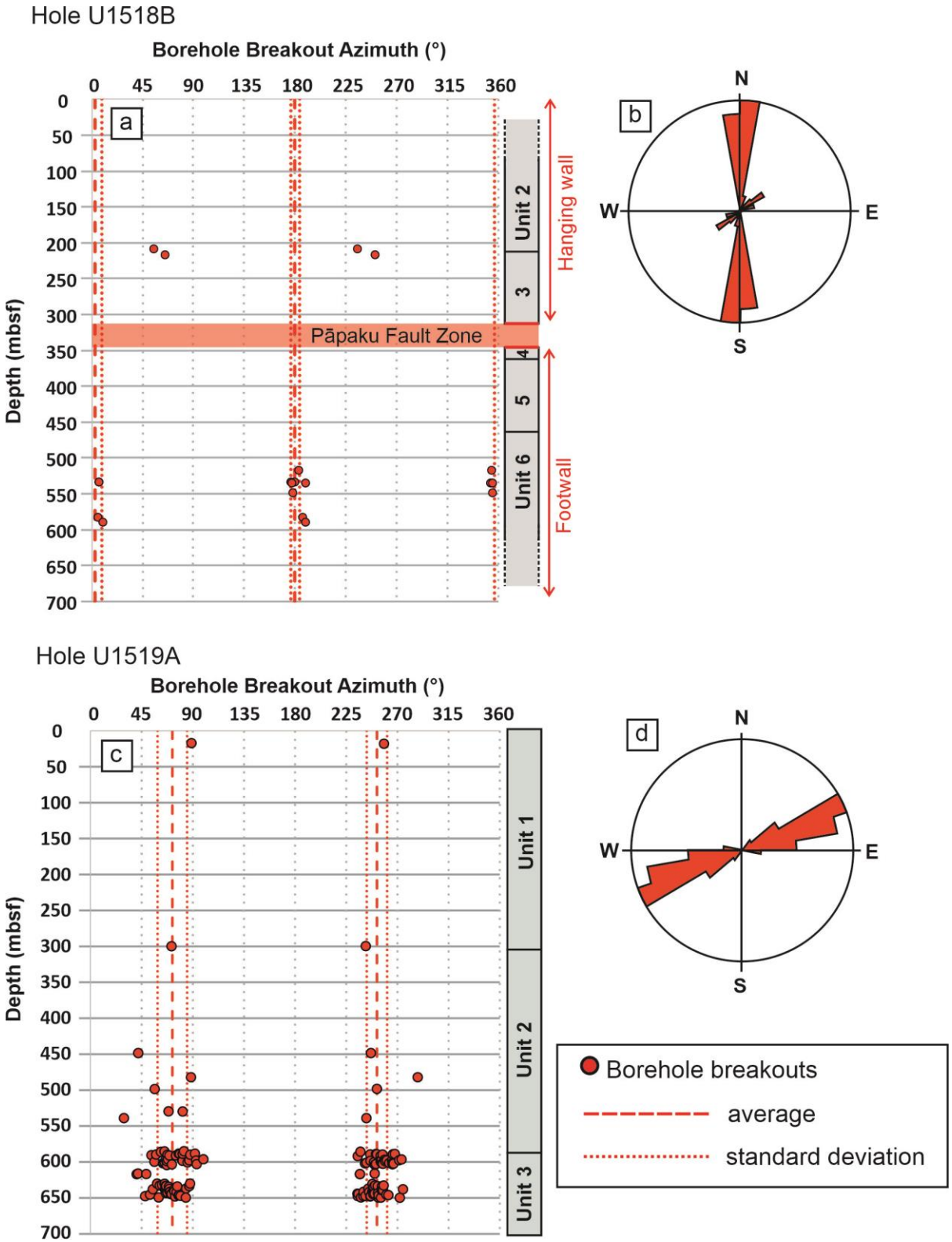

Figure 2 a) Borehole breakout azimuth as a function of depth (mbsf) in Hole U1518B. Depth extent of the Pāpaku Fault and LWD-defined units shown on the right (Cook et al., 2020; Saffer et al., 2019a), b) Bi-directional rose diagram of Hole U1518B borehole breakout azimuths, c) Borehole breakout azimuth in Hole U1519A as a function of depth (mbsf). LWD-defined units shown on the right Barnes et al., 2019), d) Bi-directional rose diagram of Hole U1519A borehole breakout azimuths.

4 Discussion

The stress orientation data presented here are the first direct measurements made across the offshore northern HSM (Figure 3). At the borehole scale, S_{Hmax} rotates from an E-W orientation at the Pāpaku fault, an active thrust fault splay near the deformation front (Site U1518), to a NNW-SSE orientation above the plate interface where peak slip in SSEs occurs (Site U1519), and finally to a NE-SW orientation in onshore wells (Figure 3). Geological and tectonic influences on stress direction variability at both the well scale and across the northern HSM are discussed here.

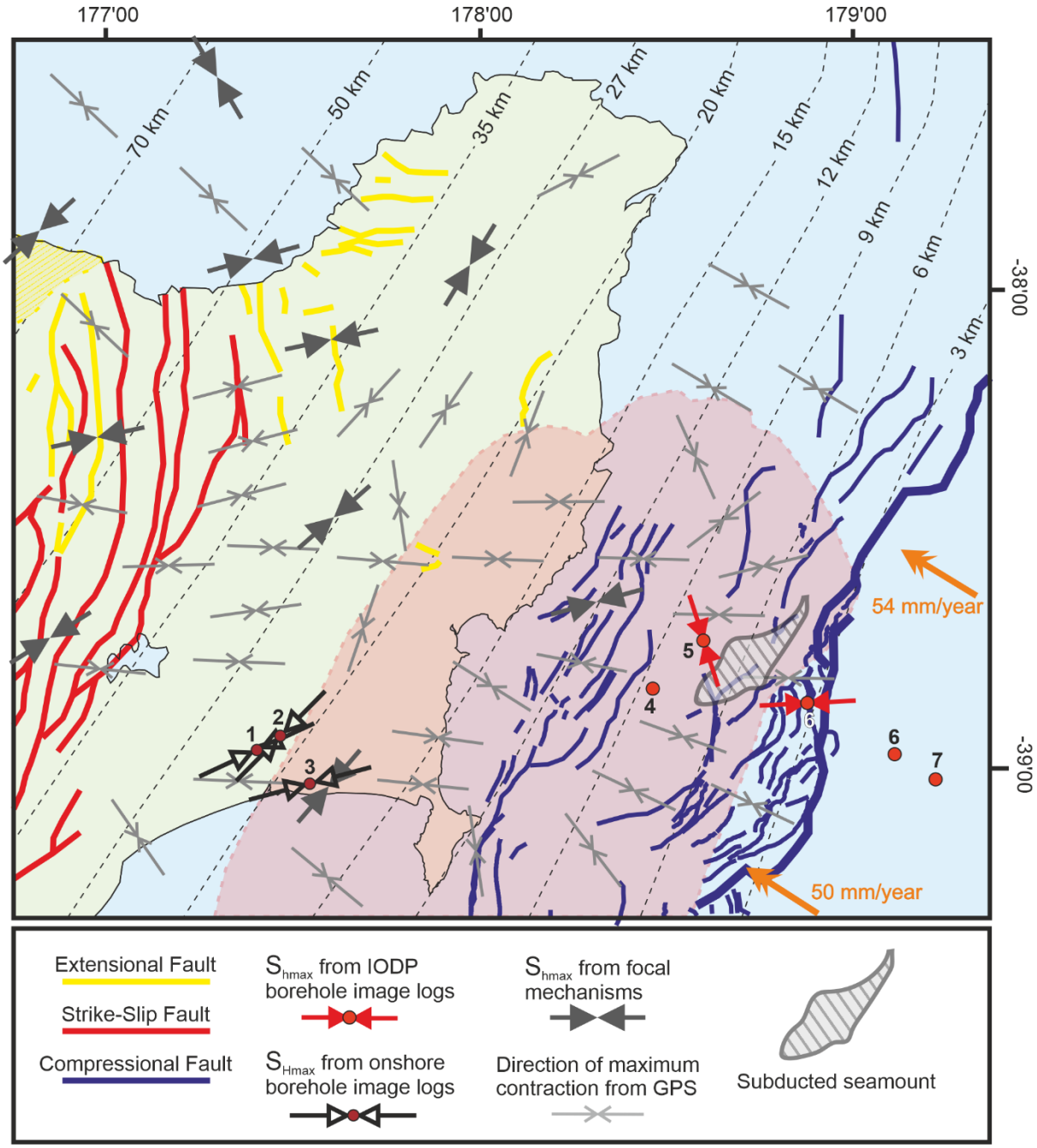

Figure 3. Map of the northern HSM showing S_{Hmax} orientations from IODP borehole image logs, borehole image analysis from (Lawrence, 2018), and focal mechanism S_{Hmax} from (Townend et al., 2012). Also shown is the direction of maximum contraction from GPS (Haines & Wallace, 2020). Plate convergence direction (orange arrows) and rate obtained from (Laura M. Wallace et al., 2012). Wells are numbered (1 – Kauhauroa-2, 2 – Kauhauroa-5, 3 – Tuhara-1A, 4 – U1517, 5 – U1519A, 6 – U1518B, 7 – U1520B, 8 – U1526). Thin, dashed, black lines show depth contours to the subduction interface (Williams et al., 2013), and the transparent red zone is the extent of cumulative slow slip in the northern HSM occurring between 2002-2012 (Wallace et al., 2012). Faults traces from (Barnes et al., 2010; Langridge et al., 2016; Mountjoy & Barnes, 2011; Pedley et al., 2010).

4.1 Well-scale stress orientation variability at Sites U1518 and U1519

The rotation of S_{Hmax} within Hole U1518B from NW-SE direction in the Pāpaku Fault hanging wall to E-W in the footwall is indicated by a small number of data points. This depth-related stress rotation, if real, may be explained by a number of processes acting in combination or separately. First, as the Pāpaku Fault is an active splay fault near the trench, recent slip on this structure may have perturbed the stress field. Second, the NW-SE S_{Hmax} orientation is observed within a depth interval of core-scale hanging wall folds and fractures (Fagereng et al., 2019). LWD resistivity image logs of this same depth interval also reveal the presence of fracturing and bedding orientation patterns consistent with large-scale folding (Wallace et al., 2018). Recent slip on faults and fractures associated with this deformed depth interval may have generated a local rotation on the stress directions in this region. Third, east of Hole U1518B, there is an abrupt change in topography which may influence the formation and orientation of the shallower stress-induced wellbore failures observed here (Figure 1c; (Zoback et al., 1989). This topography may also have a broader effect on the overall observed E-W S_{Hmax} orientation observed at Site U1518. Modelling of the spatial influence of the topographical feature on local stress conditions at Site U1518, and more than two borehole breakout measurements are required in this region to confirm and explain the causes of stress rotations with depth here.

The small-scale variation in borehole breakout orientation within Hole U1519A is likely due to stress field perturbation from localised deformation in these depth intervals. This is supported by the large number of fractures and observation of deformed bedding within these depth intervals, as noted from LWD resistivity borehole imaging (Wallace et al., 2018).

4.2 Stress orientation variability across the Northern HSM

A number of geological and tectonic phenomena, either in isolation or in concert, could explain the observed S_{Hmax} orientation variability across the northern HSM, from the trench through to the onshore forearc. An E-W S_{Hmax} in the Pāpaku fault footwall (Site U1518), fits with the geological understanding of this region, and suggests that this site lies in a region characterized by horizontal compression

subparallel to relative plate convergence. An E-W S_{Hmax} orientation is further supported by the N-S strike of frontal thrust faults imaged in seismic and bathymetric data from this area (Barnes et al., 2020; Saffer et al., 2019a), and E-W shortening directions inferred from sediment magnetic susceptibility anisotropy measured from the Pāpaku Fault footwall (Greve et al., 2020).

NNW-SSE orientations reported from Hole U1519A are not aligned with NE-SW S_{Hmax} (margin parallel) orientations reported from onshore wells and derived from focal mechanisms, nor with E-W S_{Hmax} orientations reported from Hole U1518B (Figure 3). Several factors may explain this discrepancy. First, Hole U1519A is located ~5km above a zone of the plate interface that experiences regular large SSEs, which is locked in-between SEE events (Wallace et al., 2010, 2016) (Figure 1c). Hole U1519A was drilled and logged during a time in-between SSE events, when the subduction plate interface was locked, and elastic strain accumulation was occurring, similar to past inter-SSE periods (Wallace et al., 2010). As stress orientations from existing onshore industry wells are located above the steadily creeping plate interface region (with no locking and minimal slow slip; Figure 1, 3), the observed difference in S_{Hmax} orientations may be related to differences in plate interface behaviour (creeping beneath the onshore region; locking and episodic SSEs offshore). This assumes that stress states at the plate interface remain broadly consistent from depth to shallow crustal levels. We also note that the broadly NE-SW orientation of the onshore S_{Hmax} observations may also be related to the position of the northern Hikurangi forearc to the east of an actively extending intra-arc rift (the Taupo Volcanic Zone). Here, the forearc is likely to be under margin-normal (southeast-directed) extension, due to the transmission of slab rollback forces across the forearc and into the extending arc region (Wallace et al., 2012).

The observed NNW-SSE S_{Hmax} orientation at Hole U1519A may also result from the influence of a subducting seamount which has been inferred between Sites U1519 and U1518 (Barker et al., 2018). Numerical modelling suggests that enhanced compression (S_{Hmax} magnitude), rotation of the S_{Hmax} orientation, and increased fault-normal stresses can be expected ahead of the landward flank of the subducting seamount, while creating an extensional stress shadow behind it (Sun et al., 2020). Given that Hole U1519A is located on the landward side of the proposed subducting seamount, and in the context of the approximate seamount morphology, this may explain the observed NNW-SSE compressional direction of S_{Hmax} here (Figure 3). This theory however would require a morphological feature at the plate interface to generate a perturbation large enough to affect the stress field at shallow levels where borehole breakouts are being measured. Furthermore, this effect would have to only apply to the leading flank and not the extensional stress shadow, in order to explain the compressional S_{Hmax} orientation at Site U1518 (which is located seaward of the seamount, in the expected stress shadow).

The borehole breakout-derived S_{Hmax} orientations recorded from Hole U1519A may represent a transient stress state associated with the current interseismic SSE

period, which may change during slow slip events. If so, stress states during SSEs in this region could either rotate the S_{Hmax} orientation, change the stress state from compressional to strike-slip or extension as a result of the small, typically <1 MPa (Ide et al., 2007; Leeman et al., 2016), stress drops associated with SSEs, or allow a combination of both. Analysis of fracture orientations from GVR image logging at Site U1519 (Supplement 2) shows a dominant NNE-SSW strike consistent with the interseismic NNW-SSE compressional S_{Hmax} direction, though multiple strike orientations seen for subordinate fractures may be more consistent with alternative stress states to the one observed at the time of drilling. These may reflect temporal rotations in S_{Hmax} orientation. If SSE stress drops reduce S_{Hmax} below the S_V magnitude, becoming σ_2 or σ_3 to create a strike-slip or extensional stress state respectively, then from calculated total S_v magnitudes of the region (Supplement 1), the interseismic S_{Hmax} magnitude would fall in the region of 16-19 MPa. Until stress orientations can be quantified during slow slip events, further fracture orientation analysis is performed, and/or quantification of the interseismic S_{Hmax} magnitude from existing data is carried out, this idea remains conjectural, though worthy of further investigation.

Overall, offshore borehole breakout-derived S_{Hmax} orientations from IODP wells (NNW-SSE, and E-W) differ from the documented NE-SW S_{Hmax} for the northern HSM from shallow depths to plate interface (Lawrence, 2018; Townend et al., 2012). This may reflect a transition from a thrust fault regime in margin-normal compression at the northern HSM deformation front, to extensional (normal-faulting) and strike-slip tectonics in the onshore forearc of the northern HSM forearc, adjacent to the actively extending Taupo Volcanic Zone. We suggest that the offshore IODP stress orientations presented here are influenced by processes occurring near the deformation front, including topographical effects, possible temporal effects associated with the SSE cycle, and spatial effects associated with the presence of a subducting seamount in the region.

5 Conclusions

Changes in horizontal stress orientations are observed in a transect across the northern Hikurangi subduction margin. Borehole image log S_{Hmax} orientations imply margin-normal (E-W), maximum compression in the Pāpaku thrust fault footwall, a compressional NNE-SSW orientation in the forearc offshore Tuaheni Basin, and a NE-SW, strike-slip orientation further landward within the onshore forearc. The NNW-SSE S_{Hmax} observed ~40 km east of the coast at Site U1519 may reflect a number of offshore subduction-related processes including temporal variations in subduction interface locking and elastic strain accumulation associated with the SSE cycle, and/or spatial controls associated with subducting seamounts in this region. Well-scale variations in stress orientation are likely caused by a combination of topographic effects and recent activity on active fractures and faults.

Acknowledgements

This research used data provided by the International Ocean Discovery Program (IODP). We gratefully acknowledge IODP, Texas A&M University staff, Schlumberger Drilling and Measurements, the crew of the Joides Resolution, and the Expedition 375 and 372 science parties. D. D. McNamara is funded by Geological Survey Ireland for this work. M. Paganoni is funded by NERC grant NE/R016615/1. L. Wallace, P. Barnes, and I. Pecher acknowledge funding from the New Zealand Ministry for Business, Innovation, and Employment's Endeavour fund (contract CO5X1605 to GNS Science). A.F. acknowledges funding from ERC Horizon 2020 Starting Grant 715836. K. E. Petronotis and L. J. LeVay received funding from the IODP JRSO (NSF Grant 1326927). This work was carried out in part using the Techlog Wellbore Software provided for research purposes by Schlumberger Limited.

Acknowledgements

The well data used in this paper can accessed through IODP's database (http://mlp.ldeo.columbia.edu/ logdb/scientific_ocean_drilling/).

References

Allmann, B. P., & Shearer, P. M. (2009). Global variations of stress drop for moderate to large earthquakes. *Journal of Geophysical Research: Solid Earth*, *114*(B1). https://doi.org/10.1029/2008jb005821

Anderson, E. M. (1906). The Dynamics of Faulting. *The Journal of Geology*, *14*(3), 254–257. https://doi.org/10.1086/621305

Araki, E., Saffer, D. M., Kopf, A. J., Wallace, L. M., Kimura, T., Machida, Y., et al. (2017). Recurring and triggered slow-slip events near the trench at the Nankai Trough subduction megathrust. *Science*, *356*(6343), 1157–1160. https://doi.org/10.1126/science.aan3120

Barker, D. H. N., Henrys, S., Tontini, F. C., Barnes, P. M., Bassett, D., Todd, E., & Wallace, L. (2018). Geophysical Constraints on the Relationship Between Seamount Subduction, Slow Slip, and Tremor at the North Hikurangi Subduction Zone, New Zealand. *Geophysical Research Letters*, *45*(2), 12. https://doi.org/10.1029/2018gl080259

Barnes, P M, Wallace, L. M., Saffer, D. M., Pecher, I. A., Petronotis, K. E., LeVay, L. J., et al. (2019). Proceedings of the International Ocean Discovery Program. https://doi.org/10.14379/iodp.proc.372b375.105.2019

Barnes, Philip M, Lamarche, G., Bialas, J., Henrys, S., Pecher, I., Netzeband, G. L., et al. (2010). Tectonic and geological framework for gas hydrates and cold seeps on the Hikurangi subduction margin, New Zealand. *Marine Geology*, *272*(1–4), 26–48. https://doi.org/10.1016/j.margeo.2009.03.012

Barnes, Philip M., Wallace, L. M., Saffer, D. M., Bell, R. E., Underwood, M. B., Fagereng, A., et al. (2020). Slow slip source characterized by lithological and geometric heterogeneity. *Science Advances*, *6*(13), eaay3314. https://doi.org/10.1126/sciadv.aay3314

Beanland, S., & Haines, J. (1998). The kinematics of active deformation in the North Island, New Zealand, determined from geological strain rates. *New Zealand Journal of Geology and Geophysics*, *41*(4), 311–323. https://doi.org/10.1080/00288306.1998.9514813

Brocher, T. M. (2005). Empirical Relations between Elastic Wavespeeds and Density in the Earth's Crust. *Bulletin of the Seismological Society of America*, *95*(6), 2081–2092. https://doi.org/10.1785/0120050077

Brodsky, E. E., Saffer, D., Fulton, P., Chester, F., Conin, M., Huffman, K., et al. (2017). The postearthquake stress state on the Tohoku megathrust as constrained by reanalysis of the JFAST breakout data. *Geophysical Research Letters*, *44*(16), 8294–8302. https://doi.org/10.1002/2017gl074027

Burgreen-Chan, B., Meisling, K. E., & Graham, S. (2016). Basin and petroleum system modelling of the East Coast Basin, New Zealand: a test of overpressure scenarios in a convergent margin. *Basin Research*, *28*(4), 536–567. https://doi.org/10.1111/bre.12121

Byrne, T. B., Lin, W., Tsutsumi, A., Yamamoto, Y., Lewis, J. C., Kanagawa, K., et al. (2009). Anelastic strain recovery reveals extension across SW Japan subduction zone. *Geophysical Research Letters*, *36*(23). https://doi.org/10.1029/2009gl040749

Chang, C., McNeill, L. C., Moore, J. C., Lin, W., Conin, M., & Yamada, Y. (2010). In situ stress state in the Nankai accretionary wedge estimated from borehole wall failures. *Geochemistry*, *11*(1), Q0AD04. https://doi.org/10.1029/2010gc003261

Cook, A. E., Paganoni, M., Clennell, M. B., McNamara, D. D., Nole, M., Wang, X., et al. (2020). Physical Properties and Gas Hydrate at a Near-Seafloor Thrust Fault, Hikurangi Margin, New Zealand. *Geophysical Research Letters*, *47*(16). https://doi.org/10.1029/2020gl088474

Darby, D., & Funnell, R. H. (2001). Overpressure associated with a convergent plate margin: East Coast Basin, New Zealand. *Petroleum Geoscience*, *7*(3), 291–299. https://doi.org/10.1144/petgeo.7.3.291

Davis, E. E., Villinger, H., & Sun, T. (2015). Slow and delayed deformation and uplift of the outermost subduction prism following ETS and seismogenic slip events beneath Nicoya Peninsula, Costa Rica. *Earth and Planetary Science Letters*, *410*, 117–127. https://doi.org/10.1016/j.epsl.2014.11.015

Dimitrova, L., Wallace, L., Haines, A., & Williams, C. (2016). High-resolution view of active tectonic deformation along the Hikurangi subduction margin and the Taupo Volcanic Zone, New Zealand. *New Zealand Journal of Geology and Geophysics*, *59*(1), 43–57. https://doi.org/10.1080/00288306.2015.1127823

Dixon, T. H., Jiang, Y., Malservisi, R., McCaffrey, R., Voss, N., Protti, M., & Gonzalez, V. (2014). Earthquake and tsunami forecasts: Relation of slow slip events to subsequent earthquake

rupture. *Proceedings of the National Academy of Sciences*, *111*(48), 17039–17044. https://doi.org/10.1073/pnas.1412299111

Doser, D. I., & Webb, T. H. (2003). Source parameters of large historical (1917–1961) earthquakes, North Island, New Zealand. *Geophysical Journal International*, *152*(3), 795–832. https://doi.org/10.1046/j.1365-246x.2003.01895.x

Duan, B. (2010). Role of initial stress rotations in rupture dynamics and ground motion: A case study with implications for the Wenchuan earthquake. *Journal of Geophysical Research: Solid Earth (1978–2012)*, *115*(B5). https://doi.org/10.1029/2009jb006750

Fagereng, A., Savage, H. M., Morgan, J. K., Wang, M., Meneghini, F., Barnes, P. M., et al. (2019). Mixed deformation styles observed on a shallow subduction thrust, Hikurangi margin, New Zealand. *Geology*, *47*(9), 872–876. https://doi.org/10.1130/g46367.1

Greve, A., Kars, M., Zerbst, L., Stipp, M., & Hashimoto, Y. (2020). Strain partitioning across a subduction thrust fault near the deformation front of the Hikurangi subduction margin, New Zealand: A magnetic fabric study on IODP Expedition 375 Site U1518. *Earth and Planetary Science Letters*, *542*, 116322. https://doi.org/10.1016/j.epsl.2020.116322

Haines, A. J., & Wallace, L. M. (2020). New Zealand-Wide Geodetic Strain Rates Using a Physics-Based Approach. *Geophysical Research Letters*, *47*(1). https://doi.org/10.1029/2019gl084606

Hardebeck, J. L., & Okada, T. (2018). Temporal Stress Changes Caused by Earthquakes: A Review. *Journal of Geophysical Research: Solid Earth*, *123*(2), 1350–1365. https://doi.org/10.1002/2017jb014617

Heidbach, D. O. (2016). *WSM quality ranking scheme, database description and analysis guidelines for stress indicator* (pp. 1–55).

Hirose, H., Hirahara, K., Kimata, F., Fujii, N., & Miyazaki, S. (1999). A slow thrust slip event following the two 1996 Hyuganada Earthquakes beneath the Bungo Channel, southwest Japan. *Geophysical Research Letters*, *26*(21), 3237–3240. https://doi.org/10.1029/1999gl010999

Huffman, K. A., & Saffer, D. M. (2016). In situ stress magnitudes at the toe of the Nankai Trough Accretionary Prism, offshore Shikoku Island, JapanIn situ stress magnitudes at the toe of the Nankai Trough Accretionary Prism, offshore Shikoku Island, Japan. *Journal of Geophysical Research: Solid Earth*, *121*(2), 1202–1217. https://doi.org/10.1002/2015jb012415

Huffman, K. A., Saffer, D. M., & Dugan, B. (2016). In situ stress magnitude and rock strength in the Nankai accretionary complex: a novel approach using paired constraints from downhole data in two wells. *Earth, Planets and Space*, *68*(1), 1–9. https://doi.org/10.1186/s40623-016-0491-4

Ide, S., Beroza, G. C., Shelly, D. R., & Uchide, T. (2007). A scaling law for slow earthquakes. *Nature*, *447*(7140), 76–79. https://doi.org/10.1038/nature05780

Ito, T., & Zoback, M. D. (2000). Fracture permeability and in situ stress to 7 km depth in the KTB scientific drillhole. *Geophysical Research Letters*, *27*(7), 1045–1048. https://doi.org/10.1029/1999gl011068

Langridge, R. M., Ries, W. F., Litchfield, N. J., Villamor, P., Dissen, R. J. V., Barrell, D., et al. (2016). The New Zealand Active Faults Database. *New Zealand Journal of …*, *59*(1), 86–96. https://doi.org/10.1080/00288306.2015.1112818

Lawrence, M. J. F. (2018). *Structural and Sedimentological Interpretation of Well Data from the Wairoa Area, North Island, New Zealand* (GNS Science Report No. 2018/28) (pp. 1–84).

Leeman, J. R., Saffer, D. M., Scuderi, M. M., & Marone, C. (2016). Laboratory observations of slow earthquakes and the spectrum of tectonic fault slip modes. *Nature Communications*, *7*(1), 11104. https://doi.org/10.1038/ncomms11104

Lin, W., Yeh, E.-C., Hung, J.-H., Haimson, B., & Hirono, T. (2009). Localized rotation of principal stress around faults and fractures determined from borehole breakouts in hole B of the Taiwan Chelungpu-fault Drilling Project (TCDP). *Tectonophysics*, *482*(1), 82–91. https://doi.org/10.1016/j.tecto.2009.06.020

Lin, W., Byrne, T. B., Kinoshita, M., McNeill, L. C., Chang, C., Lewis, J. C., et al. (2015). Distribution of stress state in the Nankai subduction zone, southwest Japan and a comparison with Japan Trench. *Tectonophysics*, *692*, 1–12. https://doi.org/10.1016/j.tecto.2015.05.008

Magee, M. E., & Zoback, M. D. (1993). Evidence for a weak interplate thrust fault along the northern Japan subduction zone and implications for the mechanics of thrust faulting and fluid expulsion. *Geology*, *21*(9), 809. https://doi.org/10.1130/0091-7613(1993)021<0809:efawit>2.3.co;2

Mardia, K. V. (1975). Statistics of Directional Data. *Journal of the Royal Statistical Society: Series B (Methodological)*, *37*(3), 349–371. https://doi.org/10.1111/j.2517-6161.1975.tb01550.x

McNamara, D. D., Massiot, C., & Lewis, B. (2015). Heterogeneity of structure and stress in the Rotokawa Geothermal Field, New Zealand. *Journal of Geophysical Research, 120, 1243-1262.* https://doi.org/10.1002/(issn)2169-9356

McNamara, D. D., Milicich, S. D., Massiot, C., Villamor, P., McLean, K., Sepulveda, F., & Ries, W. F. (2019). Tectonic Controls on Taupo Volcanic Zone Geothermal Expression: Insights From Te Mihi, Wairakei Geothermal Field. *Tectonics*, *147*(1), 71–23. https://doi.org/10.1029/2018tc005296

Miller, D. J., & Dunne, T. (1996). Topographic perturbations of regional stresses and consequent bedrock fracturing. *Journal of Geophysical Research: Solid Earth*, *101*(B11), 25523–25536. https://doi.org/10.1029/96jb02531

Mountjoy, J. J., & Barnes, P. M. (2011). Active upper plate thrust faulting in regions of low plate interface coupling, repeated slow slip events, and coastal uplift: Example from the Hikurangi Margin, New Zealand. *Geochemistry*, *12*(1), Q01005. https://doi.org/10.1029/2010gc003326

Obara, K., Hirose, H., Yamamizu, F., & Kasahara, K. (2004). Episodic slow slip events accompanied by non-volcanic tremors in southwest Japan subduction zone. *Geophysical Research Letters*, *31*(23). https://doi.org/10.1029/2004gl020848

514 Pecher, I. A., Barnes, P. M., LeVay, L. J., & Scientists, E. 372A. (2019). Creeping Gas Hydrate Slides.
515 Proceedings of the International Ocean Discovery Program, 372A. *International Ocean Discovery*
516 *Program*. https://doi.org/10.14379/iodp.proc.372a.2019

517 Pedley, K. L., Barnes, P. M., Pettinga, J. R., & Lewis, K. B. (2010). Seafloor structural geomorphic
518 evolution of the accretionary frontal wedge in response to seamount subduction, Poverty
519 Indentation, New Zealand. *Marine Geology*, *270*(1–4), 119–138.
520 https://doi.org/10.1016/j.margeo.2009.11.006

521 Saffer, D. M., Wallace, L. M., Barnes, P. M., Pecher, I. A., Petronotis, K. E., LeVay, L. J., et al. (2019a).
522 Proceedings of the International Ocean Discovery Program.
523 https://doi.org/10.14379/iodp.proc.372b375.103.2019

524 Saffer, D. M., Wallace, L. M., Barnes, P. M., Pecher, I. A., Petronotis, K. E., LeVay, L. J., et al. (2019b).
525 Proceedings of the International Ocean Discovery Program - Expedition 372B/375 Summary.
526 https://doi.org/10.14379/iodp.proc.372b375.101.2019

527 Sibson, R., Ghisetti, F., & Ristau, J. (2011). Stress Control of an Evolving Strike-Slip Fault System
528 during the 2010–2011 Canterbury, New Zealand, Earthquake Sequence. *Seismological Research*
529 *Letters*, *82*(6), 824–832. https://doi.org/10.1785/gssrl.82.6.824

530 Song, I., Saffer, D. M., & Flemings, P. B. (2011). Mechanical characterization of slope sediments:
531 Constraints on in situ stress and pore pressure near the tip of the megasplay fault in the Nankai
532 accretionary complex. *Geochemistry, Geophysics, Geosystems*, *12*(8), n/a-n/a.
533 https://doi.org/10.1029/2011gc003556

534 Sun, T., Saffer, D., & Ellis, S. (2020). Mechanical and hydrological effects of seamount subduction on
535 megathrust stress and slip. *Nature Geoscience*, *13*(3), 249–255. https://doi.org/10.1038/s41561-
536 020-0542-0

537 Tingay, M., Reinecker, J., & Müller, B. (2008). Borehole breakout and drilling-induced fracture
538 analysis from image logs. *World Stress Map Project*.

539 Tingay, M. R. P., Hillis, R. R., Morley, C. K., Swarbrick, R. E., & Okpere, E. C. (2003). Variation in
540 vertical stress in the Baram Basin, Brunei: tectonic and geomechanical implications. *Marine and*
541 *Petroleum Geology*, *20*(10), 1201–1212. https://doi.org/10.1016/j.marpetgeo.2003.10.003

542 Townend, J., Sherburn, S., Arnold, R., Boese, C., & Woods, L. (2012). Three-dimensional variations in
543 present-day tectonic stress along the Australia-Pacific plate boundary in New Zealand. *Earth and*
544 *Planetary Science Letters*, *353*(J. Geophys. Res. 106 2001), 47–59.
545 https://doi.org/10.1016/j.epsl.2012.08.003

546 Wallace, L M, Saffer, D. M., Barnes, P. M., Pecher, I. A., Petronotis, K. E., LeVay, L. J., et al. (2019).
547 Proceedings of the International Ocean Discovery Program - Expedition 372B/375 Methods.
548 https://doi.org/10.14379/iodp.proc.372b375.102.2019

549 Wallace, L M., & Eberhart-Phillips, D. (2013). Newly observed, deep slow slip events at the central
550 Hikurangi margin, New Zealand: Implications for downdip variability of slow slip and tremor, and

relationship to seismic structure. *Geophysical Research Letters*, *40*(20), 5393–5398. https://doi.org/10.1002/2013gl057682

Wallace, L M, Beavan, J., McCaffrey, R., & Darby, D. (2004). Subduction zone coupling and tectonic block rotations in the North Island, New Zealand. *Journal of Geophysical Research: Solid Earth*, *109*(B), B12406. https://doi.org/10.1029/2004jb003241

Wallace, L M, Wallace, J. B. L. M., & Beavan, J. (2010). Diverse slow slip behavior at the Hikurangi subduction margin, New Zealand. *Journal of Geophysical Research: Solid Earth*, *115*(B), B12402. https://doi.org/10.1029/2010jb007717

Wallace, L M., Beavan, J., Bannister, S., & Williams, C. (2012). Simultaneous long-term and short-term slow slip events at the Hikurangi subduction margin, New Zealand: Implications for processes that control slow slip event occurrence, duration, and migration. *Journal of Geophysical Research: Solid Earth (1978–2012)*, *117*(B11), n/a-n/a. https://doi.org/10.1029/2012jb009489

Wallace, L M, Fagereng, Å., & Ellis, S. (2012). Upper plate tectonic stress state may influence interseismic coupling on subduction megathrusts. *Geology*, *40*(10), 895–898. https://doi.org/10.1130/g33373.1

Wallace, L M, Webb, S. C., Ito, Y., Mochizuki, K., Hino, R., Henrys, S., et al. (2016). Slow slip near the trench at the Hikurangi subduction zone, New Zealand. *Science*, *352*(6286), 701–704. https://doi.org/10.1126/science.aaf2349

Wallace, L.M., Saffer, D. M., Barnes, P. M., Pecher, I. A., Petronotis, K. E., LeVay, L. J., & Scientists, E. 372/375. (2018). *Volume 372B/375 Hikurangi Subduction Margin Coring, Logging, and Observatories* (Proceedings of the International Ocean Discovery Program). International Ocean Discovery Program. Retrieved from http://publications.iodp.org/proceedings/372B_375/372B375title.html

Warren-Smith, E., Fry, B., Wallace, L., Chon, E., Henrys, S., Sheehan, A., et al. (2019). Episodic stress and fluid pressure cycling in subducting oceanic crust during slow slip. *Nature Geoscience*, *12*(6), 475–481. https://doi.org/10.1038/s41561-019-0367-x

Williams, C. A., Eberhart-Phillips, D., Bannister, S., Barker, D. H. N., Henrys, S., Reyners, M., & Sutherland, R. (2013). Revised Interface Geometry for the Hikurangi Subduction Zone, New Zealand. *Seismological Research Letters*, *84*(6), 1066–1073. https://doi.org/10.1785/0220130035

Zoback, M D, Barton, C. A., Brudy, M., Castillo, D. A., Finkbeiner, T., Grollimund, B. R., et al. (2003). Determination of stress orientation and magnitude in deep wells. *International Journal of Rock Mechanics and Mining Sciences*, *40*(7), 1049–1076. https://doi.org/10.1016/j.ijrmms.2003.07.001

Zoback, M. L., Zoback, M. D., Adams, J., Assumpção, M., Bell, S., Bergman, E. A., et al. (1989). Global patterns of tectonic stress. *Nature*, *341*(6240), 291–298. https://doi.org/10.1038/341291a0

Zoback, M D., & Townend, J. (2001). Implications of hydrostatic pore pressures and high crustal strength for the deformation of intraplate lithosphere. *Tectonophysics*, *336*(1–4), 19–30. https://doi.org/10.1016/s0040-1951(01)00091-9

Figure 1.

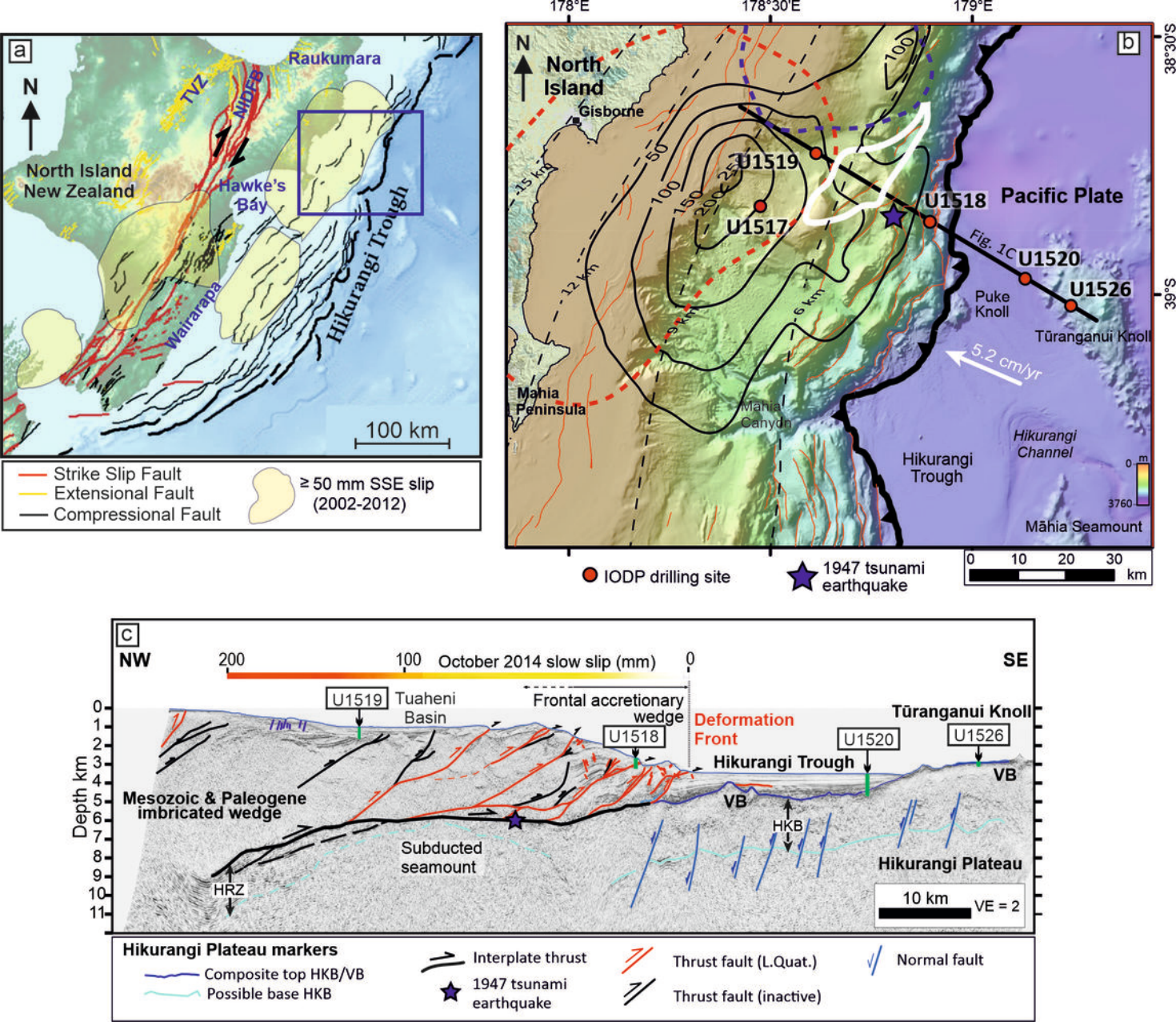
a
N
Raukumara
TVZ
NIDFB
North Island
New Zealand
Hawke's
Bay
Wairarapa
Hikurangi Trough
100 km
Strike Slip Fault
Extensional Fault
Compressional Fault
≥ 50 mm SSE slip
(2002-2012)
178°E
178°30'E
179°E
38°30'S
39°S
b
N
North
Island
Gisborne
U1519
U1517
U1518
U1520
U1526
Pacific Plate
Fig. 1C
Puke
Knoll
Tūranganui Knoll
5.2 cm/yr
Mahia
Peninsula
Mahia
Canyon
Hikurangi
Trough
Hikurangi
Channel
Māhia Seamount
15 km
12 km
9 km
6 km
100
50
150
200
250
0
m
3760
0 10 20 30
km
IODP drilling site
1947 tsunami
earthquake
c
NW
SE
200
100
October 2014 slow slip (mm)
0
U1519
Tuaheni
Basin
Frontal accretionary
wedge
U1518
Deformation
Front
U1520
U1526
Tūranganui Knoll
Hikurangi Trough
VB
VB
HKB
Mesozoic & Paleogene
imbricated wedge
Subducted
seamount
HRZ
Hikurangi Plateau
Depth km
0
1
2
3
4
5
6
7
8
9
10
11
10 km
VE = 2
Hikurangi Plateau markers
Composite top HKB/VB
Possible base HKB
Interplate thrust
1947 tsunami
earthquake
Thrust fault (L.Quat.)
Thrust fault (inactive)
Normal fault

Figure 2.

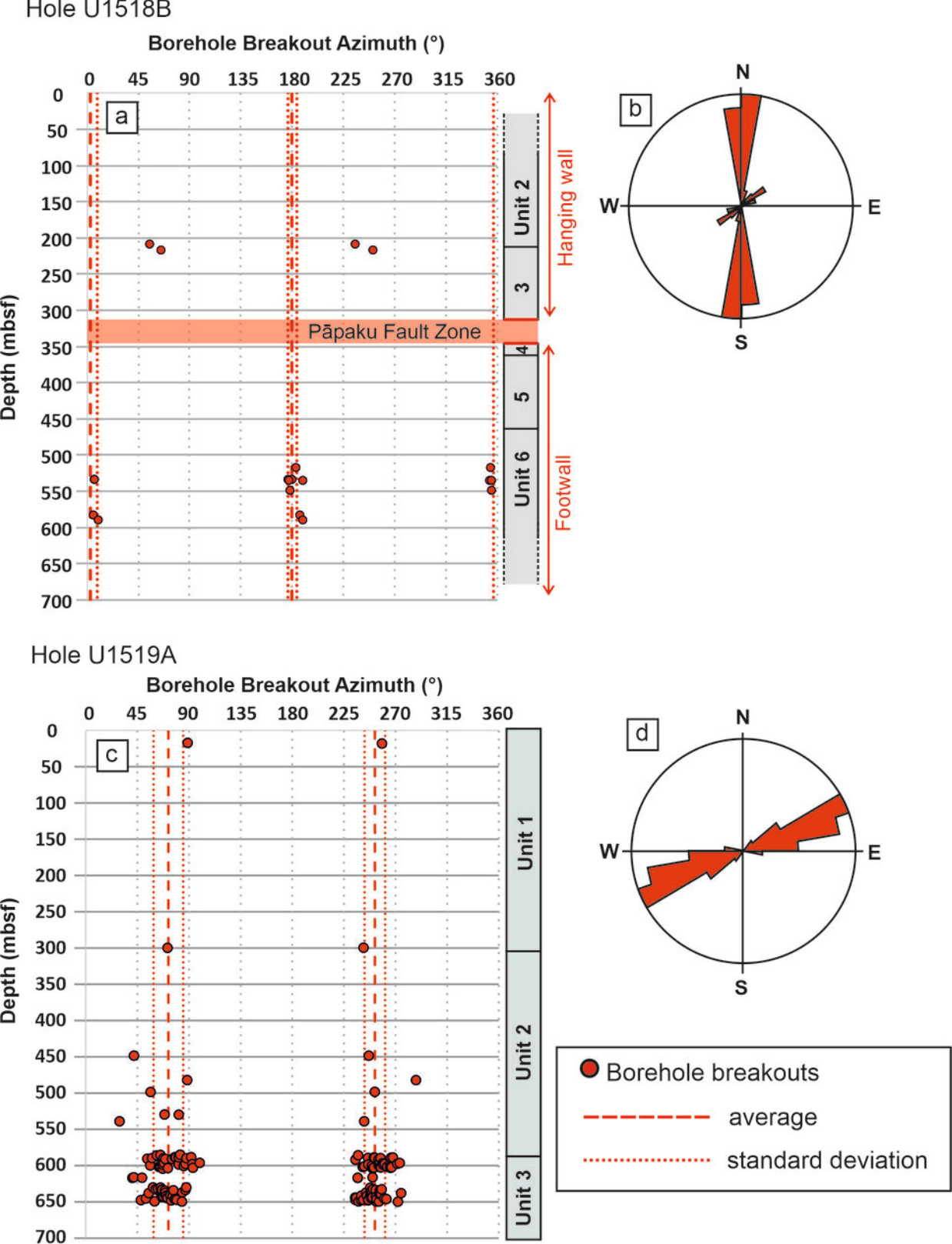
Hole U1518B
Borehole Breakout Azimuth (°)
0 45 90 135 180 225 270 315 360
a
Depth (mbsf)
0 50 100 150 200 250 300 350 400 450 500 550 600 650 700
Unit 2
3
Hanging wall
Pāpaku Fault Zone
4
5
Unit 6
Footwall
b
N
W
E
S
Hole U1519A
Borehole Breakout Azimuth (°)
0 45 90 135 180 225 270 315 360
c
Depth (mbsf)
0 50 100 150 200 250 300 350 400 450 500 550 600 650 700
Unit 1
Unit 2
Unit 3
d
N
W
E
S
Borehole breakouts
average
standard deviation

Figure 3.

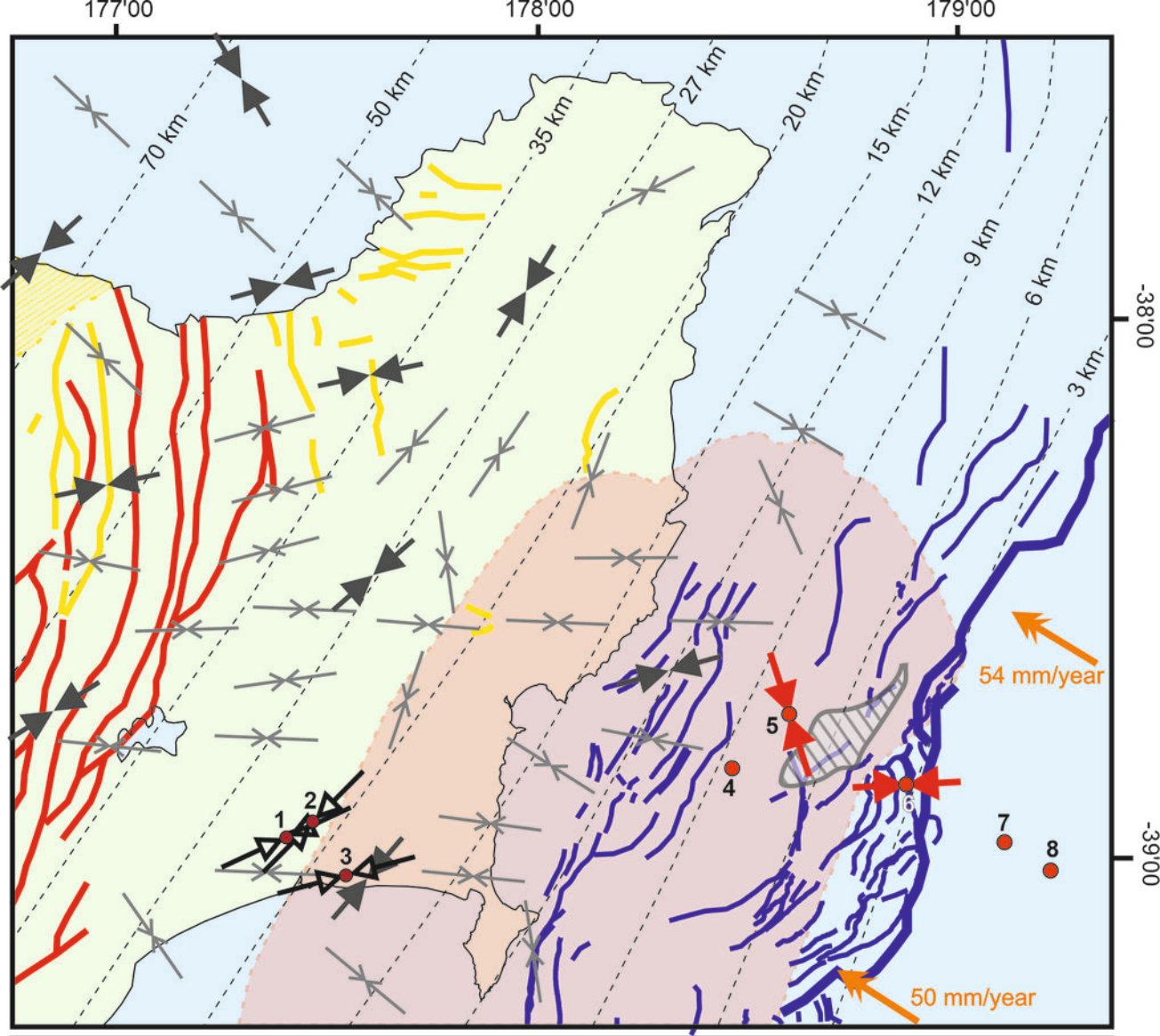
177'00
178'00
179'00
-38'00
-39'00
70 km
50 km
35 km
27 km
20 km
15 km
12 km
9 km
6 km
3 km
54 mm/year
50 mm/year
1
2
3
4
5
6
7
8
Extensional Fault
Strike-Slip Fault
Compressional Fault
S_hmax from IODP borehole image logs
S_Hmax from onshore borehole image logs
S_hmax from focal mechanisms
Direction of maximum contraction from GPS
Subducted seamount